

Contract No:

This document was prepared in conjunction with work accomplished under Contract No. DE-AC09-08SR22470 with the U.S. Department of Energy.

Disclaimer:

This work was prepared under an agreement with and funded by the U.S. Government. Neither the U. S. Government or its employees, nor any of its contractors, subcontractors or their employees, makes any express or implied: 1. warranty or assumes any legal liability for the accuracy, completeness, or for the use or results of such use of any information, product, or process disclosed; or 2. representation that such use or results of such use would not infringe privately owned rights; or 3. endorsement or recommendation of any specifically identified commercial product, process, or service. Any views and opinions of authors expressed in this work do not necessarily state or reflect those of the United States Government, or its contractors, or subcontractors.

Measurement of Wind Speed from Cooling Lake Thermal Imagery

Alfred J. Garrett, R. Cary Tuckfield, Eliel Villa Aleman, Robert J. Kurzeja, Malcolm M. Pendergast
Savannah River National Laboratory, Highway 1, Aiken, SC, USA 29808

ABSTRACT

The Savannah River National Laboratory (SRNL) collected thermal imagery and ground truth data at two commercial power plant cooling lakes to investigate the applicability of laboratory empirical correlations between surface heat flux and wind speed, and statistics derived from thermal imagery. SRNL demonstrated in a previous paper [1] that a linear relationship exists between the standard deviation of image temperature and surface heat flux. In this paper, SRNL will show that the skewness of the temperature distribution derived from cooling lake thermal images correlates with instantaneous wind speed measured at the same location. SRNL collected thermal imagery, surface meteorology and water temperatures from helicopters and boats at the Comanche Peak and H. B. Robinson nuclear power plant cooling lakes. SRNL found that decreasing skewness correlated with increasing wind speed, as was the case for the laboratory experiments. Simple linear and orthogonal regression models both explained about 50% of the variance in the skewness - wind speed plots. A nonlinear (logistic) regression model produced a better fit to the data, apparently because the thermal convection and resulting skewness are related to wind speed in a highly nonlinear way in nearly calm and in windy conditions.

Keywords: thermal imagery, wind speed, skewness, heat flux, cooling lake

1. INTRODUCTION

In a previous paper [1] a statistical analysis of 1,175 infrared radiation (*IR*) lake surface images (cells) showed a strong positive correlation between the calculated heat flux measurement (W/m^2) and the standard deviation (SD) of surface temperature measurements ($^{\circ}\text{C}$) per image. In addition, it was determined that heat flux could be modeled as a simple linear function of SD by the linear regression method known as weighted least squares [2]. However, SD is heavily influenced by wind speed which also affects lake surface patterns of heat convection and dispersion [1], and in turn will bias any estimate of heat flux.

This report presents the results of further statistical analyses to address two problems. The first was to explore the possibility of predicting wind speed solely from surface temperature measurement distribution parameters within a 2D *IR* image. The second was to estimate a value of SD per *IR* image corrected for, if possible, the predicted value of wind speed. This correction factor methodology, if successful, can then be applied to produce a more reliable estimate of heat flux among *IR* images where no concomitant measure of the actual wind speed is available. The hypothesis that wind speed correlates with the statistics of thermal images of cooling lakes was based on laboratory convection experiments by J. R. Saylor at Clemson University [3].

2. STATISTICAL ANALYSIS

Four sets of *IR* images, 699 images in all, were used to determine the effects of the prevailing wind speed across the lake surface on the corresponding heat flux. These images were obtained from two lakes - 3 sets (CP1 – CP3) from the Comanche Peak Power Plant cooling lake near Ft. Worth, Texas and 1 set (RB1) from the H. B. Robinson Power Plant cooling lake near Hartsville, South Carolina. Each image of approximately 6 m^2 of the lake surface was obtained from an *IR* camera mounted to a boat. The camera support construction allowed the camera lens to point at the lake surface at a near perpendicular angle. This floating instrument station navigated to fixed lake surface location and collected *IR* lake surface images every minute for approximately 3 hrs on each of 4 days (i.e., datasets). Concomitant wind speed (ms^{-1}) measurements were also collected from a nearby anemometer as part of a floating meteorological data collection station. Each image was subjected to a “high boost filter” (HBF) process [4] to minimize the effects of optical

distortions at the corners and near the edges of each image. The resulting image contained 49,601 pixels (193 rows by 257 columns), each pixel representing a surface temperature measurement location.

The problem of characterizing the spatial distribution of *IR* temperature measurements per image via a summary statistic was approached in two ways, viz., by the method of geostatistics and the method of moments of the empirical probability distribution. Geostatistical methods [5] were used to estimate the amount of spatial correlation for measures of antibiotic resistance and metal concentration within streams by plotting the empirical variogram ($\gamma(\mathbf{h})$), given by

$$\gamma(\mathbf{h}) = \frac{1}{2N(\mathbf{h})} \sum_{i=1}^{N(\mathbf{h})} [z(\mathbf{x}_i) - z(\mathbf{x}_i + \mathbf{h})]^2, \quad \text{for } |\mathbf{h}| > 0 \quad (1)$$

where $N(\mathbf{h})$ is the number of pairs of pixel locations with a between-location or spatial separation distance $\mathbf{h} = |\mathbf{h}|$, $z(\mathbf{x}_i)$ and $z(\mathbf{x}_i + \mathbf{h})$ are the (*IR*) temperature response measures for the i^{th} easting (x_e) and northing (x_n) coordinates for sampling location $\mathbf{x}_i = (x_e, x_n)_i$ within the image and its paired location $+\mathbf{h}$ distance units away, respectively. The emboldened letter \mathbf{h} indicates a separation vector; that is, a Euclidean distance between sampling locations in 2-space. The variogram range (r_v) parameter is defined as the minimum \mathbf{h} between sampling locations (pixels) such that the correlation between measurements for each successive measurement pair is effectively zero, and the standardized variogram $\gamma_s(\mathbf{h})$ approaches 1.0 [6]. Since $\gamma(\mathbf{h})$ increases with \mathbf{h} , the estimate of r_v is obtained by plotting

$\gamma(\mathbf{h})$ versus \mathbf{h} . When \mathbf{h} is sufficiently large, $\gamma(\mathbf{h})$ is asymptotic and the value of the *IR* measurement at \mathbf{x}_i is no longer a useful predictor of the *IR* value at $\mathbf{x}_i + \mathbf{h}$. Thus, the variation among all *IR* measurement differences at paired sampling locations $\geq r_v$ units apart is strictly random. A geostatistical variogram can be modeled to estimate r_v for a given spatial response measure. Standardized variograms were fit to *IR* measurements using a spherical model [7] to obtain estimates of r_v for each image. The spherical model is of the form

$$\gamma(\mathbf{h}) = \left\{ \begin{array}{ll} a \left[1.5 \left(\frac{\mathbf{h}}{r_v} \right) - 0.5 \left(\frac{\mathbf{h}}{r_v} \right)^3 \right] & \text{if } \mathbf{h} \leq r_v \\ a & \text{otherwise} \end{array} \right\} \quad (2)$$

where a is called the “sill” parameter and r_v the “range” parameter of the spherical model.

Spatial variograms were calculated for each *IR* image in the RB1 (124 images) data set. Visual examination of the HBF images showed a large variety of spatial patterns and shapes where clusters of similar temperatures were manifested as heat convection cells. Large rounded cloud-like cell shapes appeared to be associated with small or zero wind speeds, while “stretched” elliptical or striated patterns were associated with higher wind speeds. The sill parameter (a) is an estimate of the random variation (i.e., sample variance) among pixels sufficiently distant from one another in the image such that the spatial correlation between *IR* temperature measurements at those locations is near zero. The range parameter (r_v) of the spatial variogram is an attempt to capture these observed phenomena. It was conjectured that small ranges would accrue for cloud-like spatial patterns of convection, while large ranges would accrue for striated patterns.

The second method for characterizing spatial variation in an *IR* image was to calculate the sample moments of the empirical probability distribution (EPD) among the 49,601 *IR* temperature measurements in each image. EPD moments include the mean, mode, standard deviation (SD), skewness, kurtosis, and the inter-quartile range. They were calculated for every image in the RB1, CP1 (253 images), CP2 (197 images), and CP3 (125 images) datasets using the SAS[®] 8.02 statistical computing software from SAS Institute Inc.

These summary sample metrics of spatial variability among pixels, i.e., the variogram range and EPD moments, were thought to provide a basis for which the measured value of wind speed could be conditioned and therefore predicted.

The statistical models selected to predict wind speed are based on the least squares regression method [2] wherein wind speed was defined as a linear function of one or more of the summary sample metrics. In one instance, a nonlinear logistic regression method [8] was also used based on the data display patterns of wind speed vs. each of the summary metrics. Finally, a stepwise regression method [9] was used to produce a best fit model of wind speed as a 3rd order

polynomial function of the EPD moments fully specified with 1st order interactions terms. All regression model fits were performed using the JMP® 7.0 interactive statistical graphics software.

3. RESULTS

As shown in Figure 1, the relationship between the concomitant wind speed for each of the RB1 images and the estimated variogram range parameter r_v was positive and statistically significant ($p < .05$). This means that large values of r_v were associated with large values of wind speed, and vice versa. However, only about 10% of variability in wind speed was explained ($R^2 = .106$) by conditioning on the estimated value of r_v . Since the level of effort and cost required to produce an empirical variogram and the corresponding range parameter estimate per image, coupled with the very imprecise relationship with wind speed, this approach to the problem based on spatial statistics was abandoned in favor of an examination of the simpler and less costly method of EPD moments.

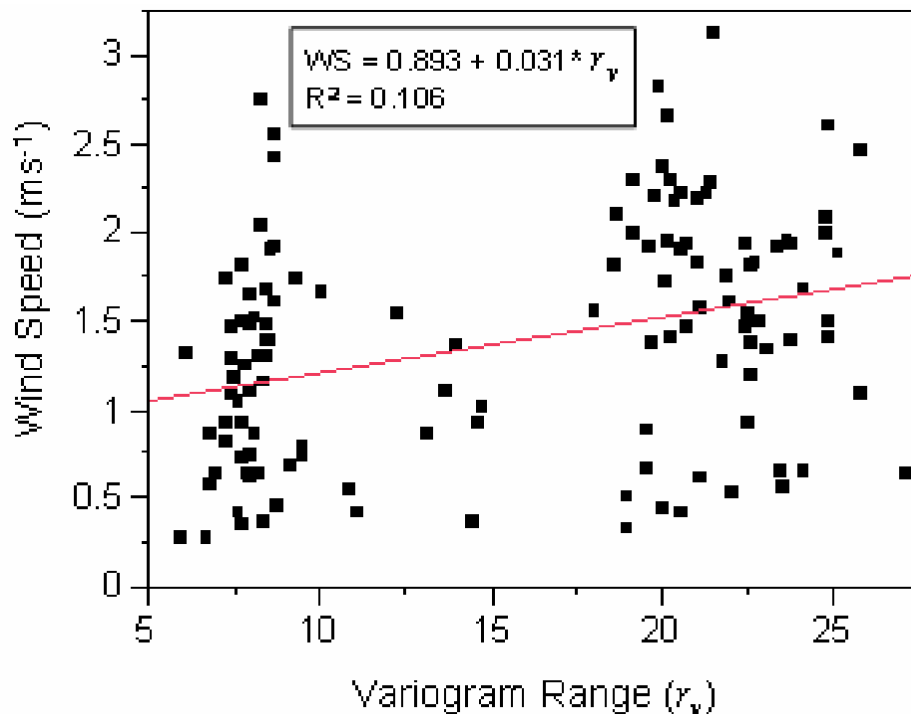


Fig. 1. Simple linear regression fit of the IR image concomitant wind speed versus the estimated variogram range parameter per image for the RB1 dataset.

The EPD moments among the 699 images from all 4 datasets could be calculated with virtually no subjectivity or judgment from the data analyst and in substantially less time than the variogram ranges.

The boxplots in Figure 2 illustrate the variation in concomitant wind speed measurements and show the disparity among data sets. Note that data for CP1-CP3 were collected on three successive days, October 30, 31, and November 1, respectively. The RB1 data were collected in the month of April. Note also that the corresponding histograms of these datasets show winds speed distributions that are negatively skewed for CP1 and positively skewed for CP2. This is not surprising since the wind speed over successively equal increments of time can be viewed and a counterpart to a well known family of probability distributions known as “waiting time” distributions. In the latter, the distribution of waiting times to a certain event, if the events occur at random, has a shape parameter in addition to a location and scale parameter. However, the values of the shape parameters in every instance are positive. Wind speed distributions, and as

it turns out, *IR* temperature measurement distributions among pixels can demonstrate both positive and negative shape (i.e., skewness) parameters. In fact, a test was performed on a single image from the CP1 dataset to determine the best fit among probability distributions using the EasyFit 5.0 software. In this single instance, the nearly 50,000 *IR* temperature measurements more closely fit a *generalized extreme value* distribution than almost all of the 39 other distributions tested.

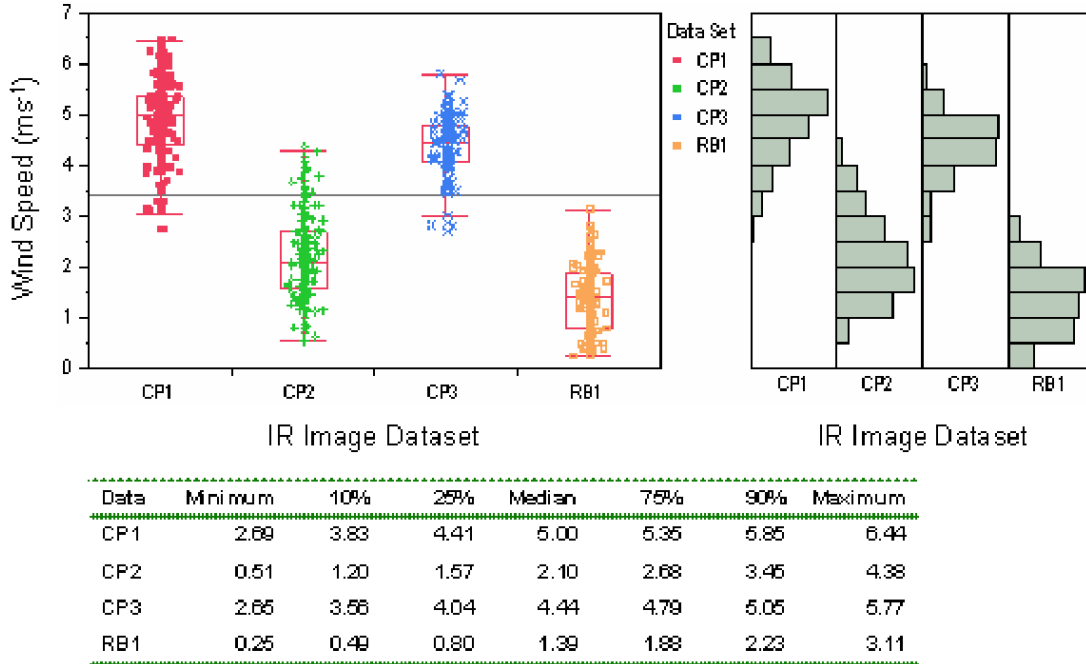


Fig. 2. Box plot and histogram data displays of wind speed measurements associated with the 699 IR images from among four images datasets (RB1, CP1, CP2, CP3). Also included are the wind speed quantiles per dataset.

Wind speed was found to be highly correlated, in fact, with two EPD moments, viz., the skewness ($r = -0.69$) and the centrality difference ($r = 0.43$) of the *IR* image temperature measurement distribution (Table 1). The latter sample moment is simply the mode minus the mean of each distribution. This measure derives from the shape of the measurement distributions as wind speed changes. When a probability distribution is symmetrical about the mean, the mode (or most frequent measurement sampled) is identical to the mean, as in a normal distribution.

Table 1. Pairwise correlation coefficients of IR image wind speed and 5 empirical probability distribution moments for 699 IR images among 4 datasets. For IR temperature measurements within each image STDINUM = standard deviation, SKINUM = skewness, KURINUM = kurtosis, QRINUM = inter-quartile range, Centrality Diff = mode – mean.

	Wind Speed	STDINUM	SKINUM	KURINUM	QRINUM	Centrality Diff
Wind Speed	1.0000	0.1583	-0.6885	0.1251	0.1613	0.4328
STDINUM	0.1583	1.0000	-0.2299	-0.0448	0.9716	-0.0032
SKINUM	-0.6885	-0.2299	1.0000	-0.3814	-0.1974	-0.5569
KURINUM	0.1251	-0.0448	-0.3814	1.0000	-0.1874	0.1354
QRINUM	0.1613	0.9716	-0.1974	-0.1874	1.0000	-0.0095
Centrality Diff	0.4328	-0.0032	-0.5569	0.1354	-0.0095	1.0000

However, with low wind speeds ($< 3 \text{ ms}^{-1}$), IR temperature measurement distributions are positively skewed, while at high wind speeds ($\geq 3 \text{ ms}^{-1}$) they are negatively skewed. This is clearly shown in Figure 3 as is also the positive relationship between wind speed and the centrality difference. The latter relation can be explained by the positive and negative values the shape parameter (skewness) of the IR temperature EPD itself. Since high wind speeds are associated with a negatively skewed distribution of IR temperature measurements, then the mode $>$ mean and the centrality difference is positive. Likewise, low wind speeds are associated with a positively skewed IR temperature distribution which means the mode $<$ mean and the centrality difference is negative (Fig. 3). Note also that the histogram of wind speed in this same scatter plot matrix (SPLOM) figure below is bimodal. This is simply the consequence of substantially overlapping distributions of IR temperature measurements between the RB1 and CP2 datasets, and the CP1 and CP3 datasets (see Figure 2), and infrequent intermediates wind speeds.

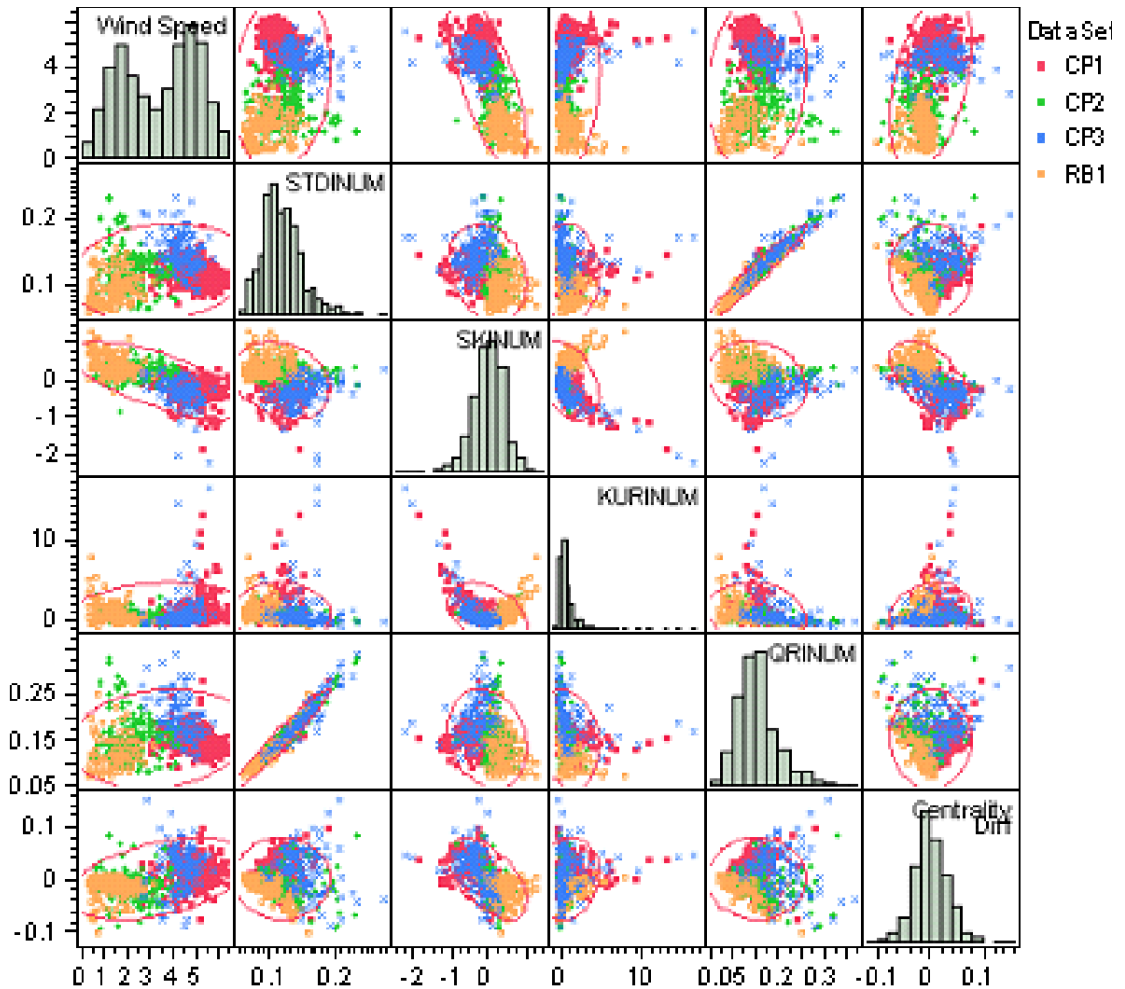


Fig. 3. Scatter Plot Matrix (SPLOM) of wind speed and 5 empirical probability distribution moments of IR temperature measurements among 4 IR image datasets (699 images total).

If we fit a simple linear regression (SLR) of wind speed to skewness, we obtain a statistically significant and negative relationship as expected with an $R^2 = .47$. However, for IR temperature measurement distributions with highly negative skewness, the corresponding predicted wind speeds from the SLR model were in excess of 10 ms^{-1} , well above the maximum of 6.5 ms^{-1} recorded during these four sampling occasions. Consequently, it was determined that a nonlinear logistic regression (NLR) model of the form

$$y_i = \frac{\theta_1}{(1 + \theta_2 e^{\theta_3 x_i})} + \varepsilon_i \quad (3)$$

where y_i is the i th wind speed measurement, x_i is the skewness parameter value of the IR temperature distribution, $\theta_1 - \theta_3$ are location, scale, and shape parameters, and ε_i is the residual error from the model fit. This model was expected to provide a better fit to these data as illustrated in Figure 4. The typical backwards S-shaped prediction curve is obtained because of the negative correlation between the response and regressor variables [8]. A better fit to the data was, in fact, obtained by the NLR model as indicated by an $R^2 = .56$. That is, an additional 10%, approximately, of the variation in wind speed was explained by an NLR model over the SLR model. Predicted wind speeds from the NLR model were more consistent with the data recorded during the field measurement activities.

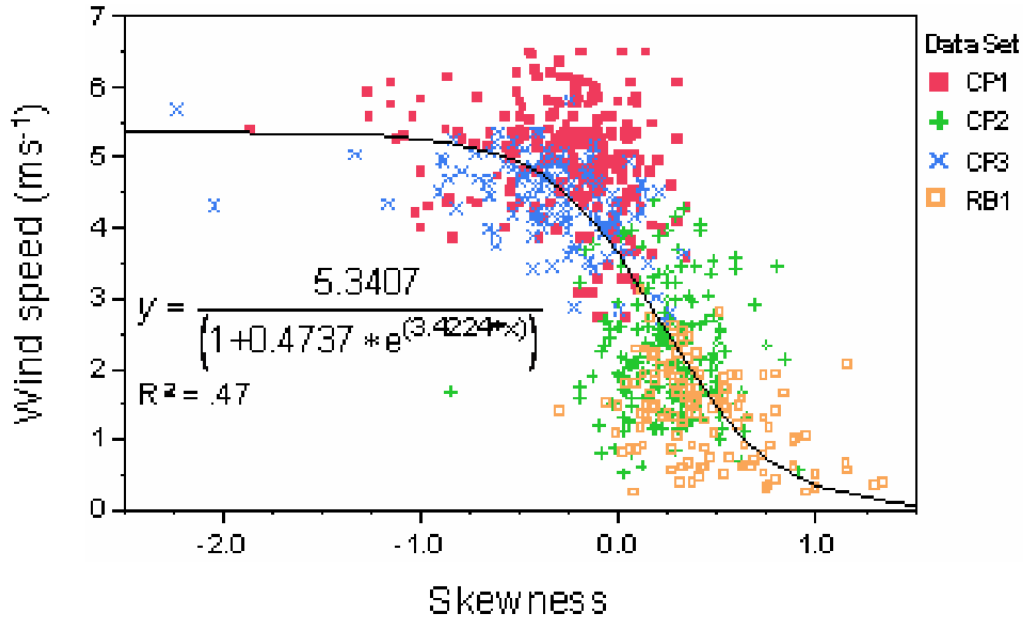


Fig. 4. Nonlinear 3-parameter logistic regression fit of the wind speed measurements versus the corresponding skewness parameter estimates per IR image..

Although a substantial improvement was achieved in wind speed prediction, it was also surmised that the methods of multiple linear regression may obtain further improvements in wind speed prediction given that other EPD moments were also correlated with wind speed. To build this model, we selected the method known as stepwise regression wherein a potential regressor variable (EPD moment) enters the model equation if and only if its significance probability (p-value) in a tested fit to wind speed is less than a specified a priori p-value or entry criterion. In a forward stepwise regression method, regressor variables (i.e., terms) enter the model one by one, or as polynomial sets, until the entry criterion is no longer met. The resulting equation for wind speed will include all model terms that make a statistically significant contribution to the model fit and therefore the R^2 statistic.

Table 2 indicates the results summary for a stepwise linear regression of wind speed using a fully specified 3rd order polynomial among 4 EPD moments, viz., skewness, kurtosis, inter-quartile range, and the centrality difference. This model is fully specified in that all six 2-way interaction terms among the 4 EPD moments were included with the polynomial terms as candidates for model inclusion. In the stepwise procedure, if a 3rd order polynomial term passes the model entry criterion, the 2nd and 1st order terms enter the model with it as a set as indicated by the number of parameters (p) in the model at each successive step (Table 2). Subsequent to this list of acceptable model terms, a standard multiple regression model was fit with all 15 (including the intercept) terms:

$$\hat{y} = \hat{\beta}_0 + \hat{\beta}_1 x_1 + \hat{\beta}_2 x_1^2 + \hat{\beta}_3 x_2 + \hat{\beta}_4 x_2^2 + \hat{\beta}_5 x_2^3 + \hat{\beta}_6 x_3^2 + \hat{\beta}_7 x_3^3 + \hat{\beta}_8 x_4 + \hat{\beta}_9 x_4^2 + \hat{\beta}_{10} x_1 x_4 + \hat{\beta}_{11} x_2 x_3 + \hat{\beta}_{12} x_3 x_4 \quad (4)$$

where

\hat{y} = wind speed

x_1 = skewness

x_2 = kurtosis

x_3 = inter-quartile range

x_4 = centrality difference

and

$\hat{\beta}_j$ = estimated values of statistical model coefficients (parameters), $j=1$ to 14

Table 2. EDP moments shown with highest statistical significance on entry to stepwise regression model at each successive step. Significance probability condition to enter the model was 0.25, and to leave was 0.10.

Step	Parameter	Action	Sig Prob	Seq SS	R ²	Cp	p
1	(SKINUM-0.0145)(SKINUM-0.0145)(SKINUM-0.0145)	Entered	0	9882	0.529	149	4
2	(QRINUM-0.15355)(QRINUM-0.15355)(QRINUM-0.15355)	Entered	0	72.99	0.568	85.53	7
3	(KURINUM-0.76355)(KURINUM-0.76355)(KURINUM-0.76355)	Entered	0	53.31	0.597	40.8	10
4	(SKINUM-0.0145)(Centrality Diff-0.00065)	Entered	0	22.94	0.609	22.97	12
5	(KURINUM-0.76355)(QRINUM-0.15355)	Entered	0.003	9.674	0.614	15.76	13
6	(QRINUM-0.15355)(Centrality Diff-0.00065)	Entered	0.052	3.981	0.616	13.97	14
7	(Centrality Diff-0.00065)(Centrality Diff-0.00065)	Entered	0.069	3.481	0.618	12.66	15

Sig Prob – significance probability of parameters (terms) to enter the model at that step; 0 = < .001

Seq SS – the reduction in the error (residual) Sum of Squares (SS) if the term is entered into the model

R² – proportion of wind speed variation explained by the regression model at the current step

Cp – Mallows' model selection criterion

p – number of parameters (terms) in the regression model, including the intercept, at the current step

Results indicate that the following wind speed prediction model with 13 terms is nearly as explanatory as the 15 term model ($R^2 = .618$) to 3 decimal places (Table 3). Thus, this multiple regression model for predicting wind speed achieves an additional 6% improvement in the amount of wind speed variation explained over and above the NLR model. Therefore, the predicted values of wind speed obtained solely from this multiple EPD moments model, may be substituted for concomitant wind speed measurements associated with an *IR* image when these actual wind speed measurements are not available.

Table 3. Summary of statistically significant EDP moments (sorted by t-Ratio) as terms in a standard multiple regression model with 12 terms plus intercept.

Term	Estimate	Std Error	t Ratio	Prob> t
SKINUM	-3.29	0.2	-16.47	0.0000
(QRINUM-0.15355)*(QRINUM-0.15355)	-214.1	21.59	-9.92	0.0000
(QRINUM-0.15355)*(QRINUM-0.15355)*(QRINUM-0.15355)	1012.1	146.2	6.92	0.0000
(SKINUM +0.01454)*(Centrality Diff-0.00065)	30.16	4.5	6.71	0.0000
(KURINUM-0.76355)*(KURINUM-0.76355)*(KURINUM-0.76355)	0.01	0	5.86	0.0000
(SKINUM +0.01454)*(SKINUM +0.01454)*(SKINUM +0.01454)	1.19	0.21	5.61	0.0000
(KURINUM-0.76355)*(KURINUM-0.76355)	-0.09	0.02	-4.29	0.0000
(QRINUM-0.15355)*(Centrality Diff-0.00065)	-60.14	25.09	-2.4	0.0168
(KURINUM-0.76355)*(QRINUM-0.15355)	-2.45	1.03	-2.38	0.0178
(Centrality Diff-0.00065)*(Centrality Diff-0.00065)	76.2	32.57	2.34	0.0196
KURINUM	0.12	0.06	2.03	0.0425
Centrality Diff	3.98	2.11	1.89	0.0598

Finally, with reasonably precise wind speed predictions (compared to the actual measurements), we are prepared to demonstrate the well known relation [1] between heat flux and SD from the IR temperature measurements among image pixels, having first corrected SD for either the actual or predicted wind speed. The correction factor [1] is required to adjust SD down in value when it otherwise would be inflated due to wind speed. Figure 5 illustrates the prediction relation by means of SLR of heat flux as a function of $SD_{(corrected)}$. The upper panel of this Figure shows the heat flux prediction relation when SD is corrected using the *actual* wind speeds while the lower panel shows the same when SD is corrected using the *predicted* wind speeds. Although the precision in estimating the heat flux suffers somewhat between these two models ($R^2 = .79$ vs $.57$, respectively) we may provide interval estimates of the predicted heat flux by calculating the upper and lower 95 % prediction limits based on the $SD_{(corrected)}$ value for some new IR image. This interval is shown as the shaded areas within each model fit and illustrates the precision in heat flux production.

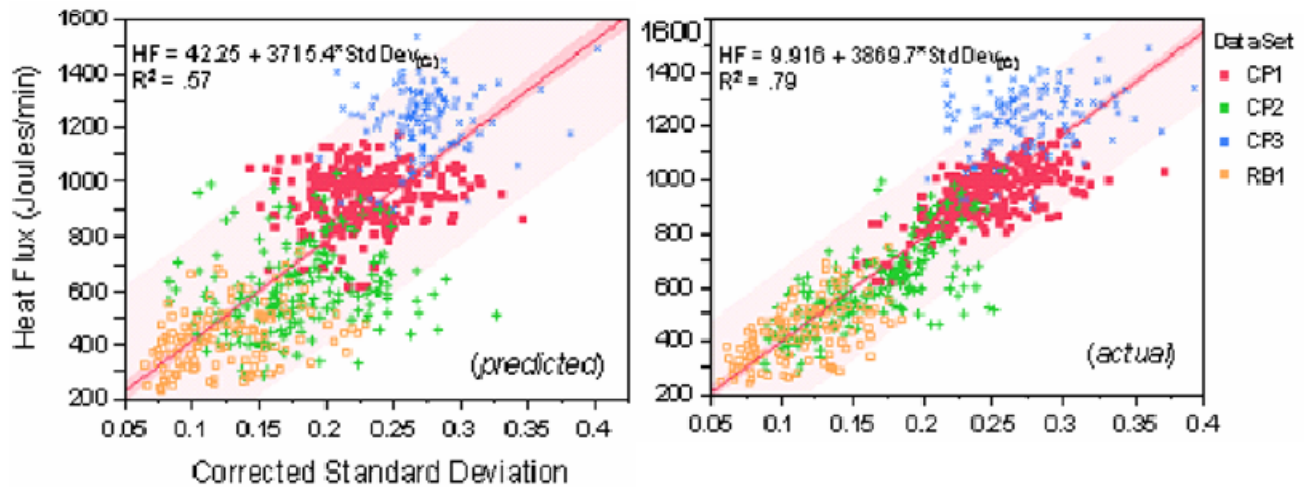


Fig. 5. Heat flux as a function of the IR temperature standard deviation per image corrected for the actual (measured) and the predicted wind speed. Predicted wind speed was derived from multiple regression of actual wind speed on EPD moments. Shaded areas show 95% prediction limits.

4. DISCUSSION

The use of spatial statistics was not without merit. The positive and statistically significant relationship between wind speed and r_v confirms what was observed by general visual inspection among the IR images, viz., that “stretched” and striated heat convection patterns were associated with higher wind speeds. In this dataset (RB1) the wind speeds only ranged from < 1 to about 3 ms^{-1} , whereas in two of the other three datasets (CP1 and CP3) maximum wind speeds were approximately 6 ms^{-1} . In other words, we would expect similar relationships between wind speed and r_v among IR images in the other datasets. But because of cost and the “artful” intervention of the user required in estimating variograms and range parameters with spatial statistics modeling software, this method does not seem practical for solving the first problem identified in this study. Perhaps the variability in wind speed as a function of r_v is related to the issues of isotropy [5]. Higher wind speeds tend to produce stretched surface patterns in the prevailing wind direction. Variograms and associated model parameter estimates produced at angles outside of this prevailing wind direction will differ substantially from those along the axis of the prevailing wind direction. When spatial variation in the response measure of interest is not the same in all directions, such a condition is known as *anisotropy*. However, at very low wind speeds the conditions of *isotropy* will obtain. Spatial variation in temperature among pixels should be direction independent and will likely derive from a random process, a process dominated by the physics of within-lake heat convection. Both spatial correlation and the variogram range therefore, should be correspondingly small.

The attractiveness for using the NLR model comes from our knowledge of the constraints in lake surface tension. Wind speeds substantially $> 6.5 \text{ ms}^{-1}$ will often produce “white caps” on the lake surface and will thwart attempts thereafter to obtain reliable IR temperature measurements. Predicted values of wind speed from the NLR model are therefore constrained to the asymptote of the nonlinear function of skewness and obtain a maximum value just $< 6 \text{ ms}^{-1}$.

The second approach to the first problem of accurately predicting wind speed is most cost effectively accomplished and with more precision by a regressing wind speed on the EPD moments of the IR temperature measurement distributions using a fully specified 3rd order polynomial model in these moments plus all 2-way among the four moments of interest. The SD is also an EPD moment, but it was excluded from the wind speed prediction analysis since it is the corrected regressor variable for predicting heat flux in our second problem. Thus, we avoided any logical circularities in correcting SD for predicted wind speed were we to use the SD to predict wind speed. Furthermore, predicted values of wind speed ranged from $0.05 - 6.5 \text{ ms}^{-1}$ which more closely matches the range of actual wind speeds among all four datasets compared to the NLR model.

ACKNOWLEDGMENTS

This report was prepared for the United States Department of Energy under Contract No. DE-AC09-96SR18500. The authors would like to thank the personnel at the H. B. Robinson and Comanche Peak power plants for their support. The authors would also like to acknowledge the insights and data provided by Professor John Saylor of Clemson University.

REFERENCES

- [1] A. J. Garrett, E. Villa-Aleman, M. M. Pendergast, R. J. Kurzeja. “Direct measurements of heat flux from cooling lake thermal imagery” SPIE Defense + Security Conference, paper 6939-28, Orlando. (2008)
- [2] Neter, J., Kutner, M. H., Nachtsheim, C. J., and Wasserman, W. [Applied Linear Statistical Models]. McGraw-Hill, Boston, MA. (1996)

- [3] J. R. Saylor. (unpublished laboratory convection experimental data).
- [4] R. C. Gonzalez, R. E. Woods. [Digital Image Processing]. Addison-Wesley Publishing Co., Reading, MA. (1992).
- [5] N. A. C. Cressie. [Statistics for Spatial Data] Wiley Series in Probability and Statistics. John Wiley and Sons, New York (1993).
- [6] Y. Pannatier. [VARIOWIN Software for Spatial Data Analysis in 2D]. Springer-Verlag, New York. 919960
- [7] Webster, R. and Oliver M. A. Geostatistics for Environmental Scientists. 2nd Ed. John Wiley & Sons, Ltd., Chichester, UK (2007).
- [8] Bates, D. M. and Watts, D. G. [Nonlinear Regression Analysis & its Applications]. Cambridge University Press, Cambridge, UK. (1988).
- [9] Draper, N. R., and Smith, H. [Applied Regression Analysis]. 3rd Ed., John Wiley & Sons Inc., New York, NY. (2003).